



Cite this: DOI: 10.1039/c8dt03211d

A selective hydrolytic and restructuring approach through a Schiff base design on a coumarin platform for “turn-on” fluorogenic sensing of Zn²⁺†

Abha Pandey,^a Sharad Kumar Asthana,^a Anand Prakash,^b Jagat Kumar Roy,^b Ida Tiwari^a and K. K. Upadhyay *^a

A new Schiff base, **CMD**, designed based on a coumarin platform was synthesized and fully characterized through single crystal X-ray diffraction studies. **CMD** underwent selective Zn²⁺-triggered hydrolysis in ethanolic medium followed by restructuring of its fragments, resulting in a “turn-on” green fluorogenic response. This response was confirmed through various physico-chemical measurements along with single crystal X-ray diffraction studies. This selective hydrolytic fluorogenic event was exploited for the successful optical detection and live cell imaging of Zn²⁺ in SiHa cells. The above restructured products were characterized as two new Schiff bases, viz. **CM** and **NSA**, of which **NSA** was highly fluorescent (green). Hence, the formation of this green fluorogenic product accounted for the above fluorogenic “turn-on” sensing of Zn²⁺ with a sub-nanomolar detection limit. Spectroscopic evidence along with mass determinations indicated that the Zn-CMD ensemble took the form of **CM-Zn-CM** in solution, supporting our above proposal of hydrolysis and restructuring. However, the X-ray diffraction studies of the Zn-CMD ensemble further revealed it to consist of **NSA** and **CM-Zn-CM'**, where **CM'** is yet another new Schiff base formed *in situ* during the process of developing single crystals.

Received 6th August 2018,
Accepted 2nd January 2019

DOI: 10.1039/c8dt03211d

rsc.li/dalton

Introduction

Zinc is second only to iron among the most biologically relevant d-metals found in human beings.¹ The amounts of zinc ranges from nM to mM in the human body.² Most Zn²⁺ ions are bound to proteins,^{3,1b} while a small part remains in fluid. Disruption in the mobility of Zn²⁺ leads to β -amyloid formation, which in turn is responsible for a number of diseases, such as Alzheimer's, ischemia, epilepsy, Parkinson's, etc.⁴ On account of the unique stereochemical flexibility of Zn²⁺, it is an essential cofactor in various enzymes and proteins.⁵ Additionally, it plays considerably important roles in a plethora of biological processes, such as gene transcription, regulation of metalloenzymes, neuronal transmission and

apoptosis.⁶ Consequently, the intracellular concentration of Zn²⁺ is quite high, on the order of 10 to 100 mM.⁷ In view of the great importance of Zn²⁺ in living systems, its recognition is very important, particularly at low levels.⁸ A large number of optical chemosensors for various types of analytes have been reported in the literature in the past few decades.⁹ Because it is highly relevant from the viewpoint of living systems, Zn²⁺ has been targeted by chemists with a variety of chemosensors.¹⁰ However, a considerable number of these chemosensors suffer from the problem of interference from one or more metal ions, viz. Mg²⁺, Ca²⁺, Cd²⁺, etc.¹¹ However, this problem has been addressed to a large extent through chemodosimetric approaches.¹² In this connection, the chemical literature incorporates a number of reports involving the quenching of >C=N isomerization/hydrolysis, leading to remarkable colour changes.¹³ A few mentionable reports in the literature were also provided by our own research group.¹⁴ The design strategy of our probe (**CMD**) is simple; 7-hydroxy, 4-methyl coumarin aldehyde was condensed with hydrazine hydrate in a 1:1 molar ratio, and the resulting product was further condensed with 4-diethylaminosalicylaldehyde, again in a 1:1 molar ratio.

The selection of *N,N*-diethyl salicylaldehyde as a constituent was based on our previous experience and that of other

^aDepartment of Chemistry, Institute of Science, Banaras Hindu University, Varanasi-221005, Uttar Pradesh, India. E-mail: drkaushalbhu@yahoo.co.in, kku@bhu.ac.in; Tel: +91542 670 2488

^bDepartment of Zoology, Institute of Science, Banaras Hindu University, Varanasi-221005, Uttar Pradesh, India

† Electronic supplementary information (ESI) available: ¹H NMR, ¹³C NMR, IR, mass spectrum of **CMD**, **NSA**, **CM**, **CM-Zn-CM** and **CM-Zn-CM'** and crystal refinement data of **CMD**, **NSA** and **CM-Zn-CM'**. CCDC 1588901, 1856059 and 1836451. For ESI and crystallographic data in CIF or other electronic format see DOI: 10.1039/c8dt03211d

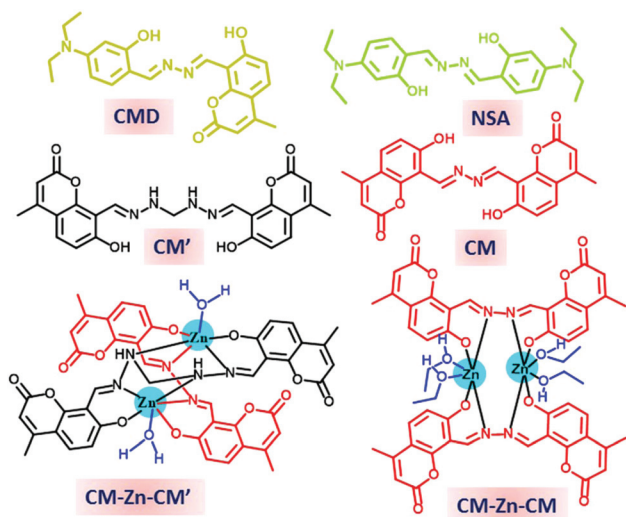


Fig. 1 Chemical structures of CMD, NSA, CM', CM, CM-Zn-CM' and CM-Zn-CM.

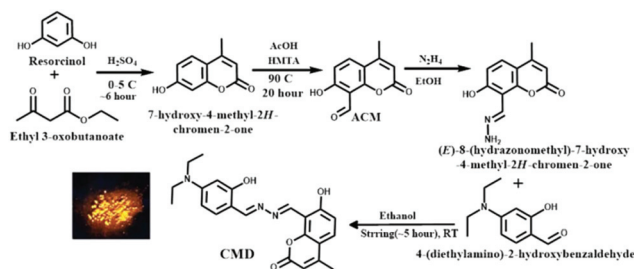
researchers regarding its multiple uses on a wide scale in the design and synthesis of chemosensors (Fig. 1).¹⁵

Zn²⁺ is a good Lewis acid in addition to being very biologically important; hence, we chose it as an analyte to examine the possibility of successful optical fluorogenic recognition by CMD. To our surprise, our strategy worked well in the sense that one highly fluorescent restructured Schiff base, *viz.* NSA, was selectively formed in due course of the interaction of CMD with Zn²⁺. This provided an indirect but foolproof method to detect the presence of Zn²⁺ in the system. This is the key step of this sensing process. At the same time, yet another restructured Schiff base, CM, was formed and ligated successfully with Zn²⁺ in a 2 : 1 molar ratio (CM-Zn-CM) with an arrangement of N₂O₄ donor sets in an octahedral geometrical pattern. Yet another structural rearrangement took place during the course of single crystal development, where one more new Schiff base, CM', was synthesized through interaction with dichloromethane, which was used for the layering. CM' coordinated with Zn²⁺ by replacing one CM in CM-Zn-CM, which ultimately resulted in the isolation of CM-Zn-CM'. Here, we observed N₃O₃ donor sets around Zn²⁺ in an octahedral geometrical pattern. Although a number of chemodosimetric approaches for analytes including Zn²⁺ have been reported in the literature, the restructuring of the fragments and the detailed characterization presented here are rare.

Experimental section

Synthesis of 4-methyl-7-hydroxy-coumarinol

First, 20.0 mmol (2.202 g) resorcinol was dissolved in 20 mL dil. sulfuric acid in a 100 mL round bottom flask; then, 25.0 mmol (~3.2 mL) ethyl acetoacetate was added to the solution with constant stirring at 0 °C to 5 °C for ~6 hours. Finally, the reaction mixture was poured into ice cold water



Scheme 1 Synthetic scheme for CMD.

(~100 mL) with stirring. The off-white precipitate thus formed was filtered and was dried in a vacuum evaporator (Scheme 1).

Spectroscopic characterization data for 4-methyl-7-hydroxy-coumarinol. Yield: 80%; M.p. 94–97 °C; IR/cm⁻¹ of CMD: 3501, 3114, 2819, 1669, 1607, 1518, 1454, 1394, 1277, 1226, 1559, 1137, 989, 848, 807, 585 (Fig. S1, ESI[†]).

Synthesis of ACM

The synthesis of ACM (7-hydroxy-4-methyl-2-oxo-2H-chromene-8-carbaldehyde) is shown in Scheme 1. In a 100 mL round bottom flask, glacial acetic acid (20.0 mL) along with 4-methyl-7-hydroxycoumarin (5.0 mmol) was taken, and hexamethylenetetramine (15.0 mmol) was added to the above reaction mixture. The reaction mixture was boiled under reflux at 80 °C to 85 °C for ~20 h. Subsequently, 5 mL of water and 30 mL dil. hydrochloric acid were added to this reaction mixture, and refluxing was continued for ~45 minutes. The reaction mixture was cooled to r.t. and was further extracted with diethyl ether. Upon evaporation of diethyl ether, a yellow solid was isolated which was further recrystallized from ethanol to afford the pure product.

Spectroscopic characterization data for ACM. Yield: 24%. M. p. 185.0–186.0 °C; IR/cm⁻¹ of ACM: 3054, 2325, 1749, 1645, 1479, 1434, 1386, 1339, 1297, 1223, 1166, 1075, 927, 897, 750, 717, 650, 591, 473, 1455, 540, 428; ¹H NMR (500 MHz, CDCl₃, TMS): δ ppm = 12.21 (s, -OH), 10.62 (s, -CHO), 7.74–7.72 (d, 1H), 6.92–6.90 (d, 1H), 6.20 (s, 1H) (Fig. S2 and S3, ESI[†]).

Synthesis of ACM-hydrazide (ACM-Hz)

(E)-8-(Hydrazonomethyl)-7-hydroxy-4-methyl-2H-chromen-2-one was synthesized by adding NH₂-NH₂·2H₂O (5.0 mmol, 160 μL) to 20 mL of a mixture of ethanol and acetic acid (2 : 1) containing ACM (0.204 g, 1.0 mM). The reaction mixture was further refluxed for ~6 h at 75 °C. The product was isolated by filtering over a sintered glass (G4) crucible. The product was washed several times with distilled water and dried under vacuum over anhydrous CaCl₂ (Scheme 1).

Spectroscopic characterization data for ACM-Hz. Yield: 70%; decomposed 241–246 °C; IR/cm⁻¹ of ACM-Hz: 3379, 3215, 1916, 1717, 1611, 2972, 2928, 1736, 1633, 1615, 1514, 1387, 1356, 1293, 1240, 1190, 1165, 1134, 1074, 1052, 936, 897, 844, 773, 705, 651, 595, 458; ¹H NMR (500 MHz, DMSO-*d*₆, TMS): δ ppm = 12.76 (s, -OH), 8.37 (s, -C=N), 7.53–7.51 (d, 1H), 7.34

(s, 2H), 6.84–6.82 (d, 1H), 6.18 (s, 1H), 2.36 (s, 3H) (Fig. S4 and S5, ESI†).

Synthesis of CMD

The synthesis of **CMD**, 8-((*E*)-((*E*)-(4-(diethylamino)-2-hydroxybenzylidene)hydrazono)methyl)-7-hydroxy-4-methyl-2*H*-chromen-2-one, is shown in Scheme 1. A 2.0 mmol absolute ethanolic solution of 4-(diethylamino)-2-hydroxybenzaldehyde was added to a separate equimolar absolute ethanolic solution of (*E*)-8-(hydrazonomethyl)-7-hydroxy-4-methyl-2*H*-chromen-2-one at room temperature for ~5 hours. A dark yellow solid was finally filtered and was dried under vacuum over anhydrous CaCl₂. **CMD** was characterized through various spectroscopic techniques such as IR, ¹H and ¹³C NMR, and ESI-mass spectral studies along with single crystal XRD analysis (Fig. S6–S9, ESI†).

Spectroscopic characterization data for receptor CMD. Yield: 70%; M.p. 224–228 °C; IR/cm⁻¹ of **CMD**: 3441, 2972, 2928, 1736, 1633, 1615, 1514, 1387, 1356, 1293, 1240, 1190, 1165, 1134, 1074, 1052, 936, 897, 844, 773, 705, 651, 595, 458; ¹H NMR (500 MHz, CDCl₃, TMS): δ ppm = 12.89 (s, -OH), 11.42 (s, -OH), 9.28 (s, -CH), 8.52 (s, -CH), 7.55–7.53 (d, -1H), 7.12–7.10 (d, -1H), 6.95–6.93 (d, -1H), 6.28–6.26 (d, -1H), 6.24 (s, 1H), 6.15 (s, -H), 3.43–3.38 (q, -4H), 2.42 (s, 3H), 1.23 (t, 6H); ¹³C NMR (125 MHz, CDCl₃) δ ppm = 164.32, 162.95, 162.21, 160.25, 155.01, 153.55, 153.00, 152.23, 134.18, 127.87, 113.79, 112.07, 111.39, 106.32, 106.23, 104.41, 97.82, 44.66, 18.90, 12.67; ESI-MS: *m/z* calculated for [C₂₂H₂₃N₃O₄] = 393.17, found = 394.3.

Synthesis of single crystals of the complex

Suitable crystals for X-ray diffraction studies of the complex were developed by slow evaporation of a saturated solution of **CMD** and **ZnOAc** prepared in 2.0 mL of a dimethylsulfoxide : ethanolic (1 : 1) mixture followed by layering with 1.0 mL dichloromethane at room temperature over a period of a few days. To our surprise, the X-ray diffraction pattern revealed the existence of two different molecular entities in the crystals. The first was identified as a new Schiff base in the form of **NSA**, while the second was identified as a zinc complex (**CM-Zn-CM'**) of yet another *in situ* synthesized Schiff base, **CM**, by Zn²⁺-triggered hydrolysis of **CMD** as well as one of its reaction products with dichloromethane (**CM'**). This *in situ* restructuring also proves the hydrolysis of **CMD** in solution (Scheme S1, ESI†).

Spectroscopic characterization data for CM-Zn-CM' + NSA. IR/cm⁻¹: 3430, 2971, 2929, 1771, 1734, 1630, 1596, 1515, 1454, 1411, 1386, 1352, 1300, 1233, 1192, 1132, 1079, 828, 788, 710, 457; ¹H NMR (500 MHz, DMSO-*d*₆, TMS): δ ppm = 11.44 (s, -OH), 9.57 (s, -C=N), 8.53 (s, -C=N, 2H), 7.66 (s, 1H), 7.22–7.21 (d, 2H), 6.25–6.23 (d, 2H), 6.048 (s, 1H), 5.96 (s, 1H), 5.65–5.63 (d, 2H), 4.58 (s, 1H), 3.33–3.30 (t, 4H), 2.46 (s, 3H), 1.08–1.05 (q, 6H); ESI-MS: *m/z* calculated for [C₂₂H₃₀N₄O₂] = 382.24, found = 383.24. [C₂₂H₁₄N₂O₆Zn] = 466.01, found = 467.18 (Fig. S10–S12, ESI†).

To verify the *in situ* synthesized products, we freshly synthesized and characterized **NSA**, **CM** and **CM-Zn-CM**.

Synthesis of NSA

NSA was synthesized by the reaction of an equimolar mixture of 4-(diethylamino)-2-hydroxybenzaldehyde and NH₂-NH₂·2H₂O according to a method previously reported by our research group.^{15a}

Spectroscopic characterization data for NSA. IR/cm⁻¹: 2972, 2929, 1628, 1593, 1557, 1515, 1485, 1453, 1414, 1375, 1352, 1300, 1228, 1132, 1080, 1014, 787, 761, 709, 650, 560; ¹H NMR (300 MHz, DMSO-*d*₆, TMS): δ ppm = ¹H NMR of **NSA** (500 MHz, DMSO-*d*₆, TMS): δ ppm = 11.45 (s, -OH), 8.56 (s, -C=N), 7.24–7.22 (d, 1H), 6.27–6.25 (d, 1H), 6.07 (s, 1H), 3.00–3.00 (q, 4H), 1.08–1.05 (t, 6H). ¹³C NMR (125 MHz, DMSO-*d*₆) δ ppm = 160.66, 160.64, 150.93, 133.03, 106.40, 104.06, 97.05, 43.87, 12.54. ESI-MS: *m/z* calculated for [C₂₂H₃₀N₄O₂] = 382.24, found = 383.15 (Fig. S13–S16, ESI†).

Synthesis of CM

The compound **CM** [((8,8'-((1*E*,1'*E*)-hydrazine-1,2-diylidenebis(methanylylidene))bis(7-hydroxy-4-methyl-2*H* chromen-2-one))] was synthesized by the reaction of an equimolar mixture of previously synthesized **ACM-HZ** and **ACM** (8-formyl-7-hydroxy-4-methyl-coumarin) in ethanol at reflux for six hours according to a previously reported method.¹⁶ **CM** was synthesized as a yellow precipitate, which was filtered and dried under vacuum.

Spectroscopic characterization data for CM. Yield: 82%; IR/cm⁻¹ of **ACM-Hz**: 3417, 3084, 2960, 1732, 1633, 1620, 1585, 1488, 1436, 1390, 1293, 1220, 1185, 1074, 936, 844, 807, 773, 457; ¹H NMR (500 MHz, DMSO-*d*₆, TMS): δ ppm = 12.72 (s, -OH), 8.40 (s, -C=N), 7.54–7.52 (d, 1H), 7.26 (s, 1H), 6.85–6.83 (d, 1H), 6.17 (s, 1H), 2.35 (s, 3H). ¹³C NMR (125 MHz, DMSO-*d*₆) δ ppm = 160.81, 160.02, 154.39, 151.39, 135.76, 125.70, 113.39, 112.21, 110.90, 107.37, 18.76; ESI-MS: *m/z* calculated for [C₂₂H₁₆N₂O₆] = 404.10, found = 405.10 (Fig. S17–S20, ESI†).

Synthesis of CM-Zn-CM

To a 10 mL ethanolic solution of **CM**, (0.404 g, 1 mmol), Zn(OAc)₂·2H₂O (0.676 g, 3 mmol) in ethanol (10 mL) was added. The yellow solution was then stirred overnight and a yellow precipitate was obtained; this was filtered and washed with a cold ethanol–water mixture (1 : 1, v/v) and dried under vacuum.

Spectroscopic characterization data for complex CM-Zn-CM. IR/cm⁻¹ of **CM-Zn-CM**: 3407, 2923, 1732, 1714, 1620, 1584, 1526, 1489, 1403, 1330, 1292, 1222, 1187, 1166, 1075, 937, 842, 816, 774, 458. ¹H NMR (500 MHz, DMSO-*d*₆, TMS): δ ppm = 8.46 (s, 1H), 7.49–7.47 (d, 1H), 6.59–6.57 (d, -1H), 5.83 (s, -1H), 1.76 (s, -3H); ¹³C NMR (125 MHz, DMSO-*d*₆) δ ppm = 174.33, 160.04, 156.55, 130.34, 120.45, 117.15, 114.44, 107.14, 106.87, 105.03, 22.75, 18.908, 18.79 (Fig. S21–S23, ESI†).

Results and discussion

X-ray diffraction studies of CMD

CMD was fully characterized through single-crystal X-ray diffraction studies. Crystals of **CMD** (Fig. 2) with suitable shapes and sizes were developed through slow evaporation of its saturated solution in dimethyl formamide over a period of 3 to 4 days. **CMD** crystallized as a monoclinic system with the space group $P2(1)/n$ (Table S1, ESI†).

The strongly fluorescent nature (orange yellow) of **CMD** in the solid state (Fig. S24, ESI†) can be attributed to a variety of non-classical intermolecular hydrogen bonds, *viz.* $N(2)\cdots H-C(1)$, $O(1)\cdots H-C(3)$ and $O(1)\cdots H-C(21A)$, with distances of separation ranging from 2.734 Å to 2.878 Å. In solution, the weakly fluorescent nature of **CMD** can be understood in terms of rupture of the above intermolecular hydrogen bonds while preserving the intramolecular hydrogen bonds between $N(1)\cdots H-O(3)$ and $N(2)\cdots H-O(4)$ with distances of separation of 1.849 Å and 1.909 Å, respectively (Fig. 3 and Fig. S25a, ESI†). These hydrogen bonds affect the availability of lone pairs over the nitrogen atoms in **CMD** for photoinduced electron transfer (PET) processes.

The torsion angle between the phenyl ring and coumarin ring of **CMD** was found to be $\sim 4^\circ$, indicating only slight non-planarity in the system (Fig. S25b†). Molecules of **CMD** underwent intermolecular $\pi\cdots\pi$ stacking involving phenyl rings in a head to tail fashion with an interseparation distance of 3.472 Å along the *a*-axis (Fig. S25c and S25d, ESI†).

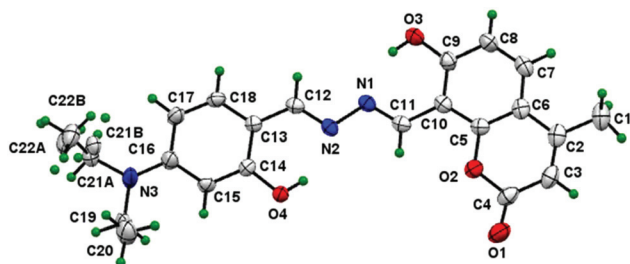


Fig. 2 ORTEP view of a single crystal of **CMD** with 50% probability.

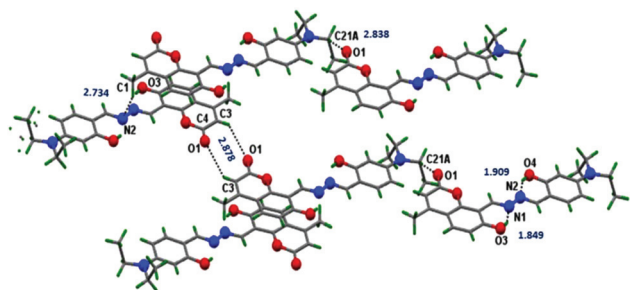


Fig. 3 Crystal structure of compound **CMD** showing stair-like packing due to non-classical hydrogen bonding.

X-ray diffraction studies of the CMD-Zn ensemble

Both obtained crystals, **NSA** and **CM-Zn-CM'**, crystallized as monoclinic systems with the space group $P21/n$ (Table S1, ESI†). The asymmetric unit of **CM-Zn-CM'** is shown in Fig. 4. A probable mechanistic description showing the genesis of **NSA**, **CM**, **CM'** and **CM-Zn-CM'** is presented in diagrammatic form in Scheme S1, ESI†.

The X-ray crystal structure of **NSA** (Fig. S26, ESI†) along with its detailed lattice parameters is given in (Table S1, ESI†); these are highly similar to the crystal details previously published by us elsewhere.^{15b}

In the crystal structure of **CM-Zn-CM'**, a number of distorted solvents were found to be present; however, these did not affect the overall structure of the complex. Most of these were subsequently removed by the PLATON/SQUEEZE tool.¹⁷ The few remaining distorted solvents were removed using Mercury software. The **CM-Zn-CM'** ensemble crystallized in the form of a binuclear complex where the interseparation distance between two zinc atoms was equal to 3.919 Å. Each Zn^{2+} has a N_3O_3 coordination atmosphere with distorted octahedral positioning. Of the two Zn, Zn(1) suffers slightly more distortion than Zn(2), which is also evident from relevant bond angle measurements: $O(1)WZn(1)O(3) = 99.9(1)$, $N(1)Zn(1)N(3) = 73.9(1)$, $O(1)WZn(1)N(6) = 157.8(1)$, $O(3)Zn(1)N(3) = 159.1(1)$, $O(10)Zn(1)N(3) = 104.3(1)$, $O(3)Zn(1)N(6) = 100.9(1)$, and $O(9)Zn(2)N(2) = 95.4(1)$. The Zn(2) center has angles $O(2)WZn(2)N(5) = 169.8(1)$, $O(4)Zn(2)O(9) = 104.7(1)$, and $O(4)Zn(2)N(2) = 158.9(1)$. Furthermore, the crystal structure also indicates considerable uplifting of both zinc atoms from the crystal plane, by 0.196 Å [Zn(1)] and 0.176 Å [Zn(2)]. This observation further substantiates the distortion in the crystal structure as discussed above.

The N_3O_3 coordination of each Zn comprises two imine nitrogens (one from **CM** and another from **CM'**) and one amine nitrogen [N(3) or N(2)] (Scheme S1, ESI†). On the other hand, of the three coordinating oxygens, two are in the form of phenolates, while the third originates from water, *i.e.* an aqua ligand. Thus, there are two aqua ligands (one per Zn^{2+} in the **CM-Zn-CM'** complexes). The Zn–O bond lengths ranged from

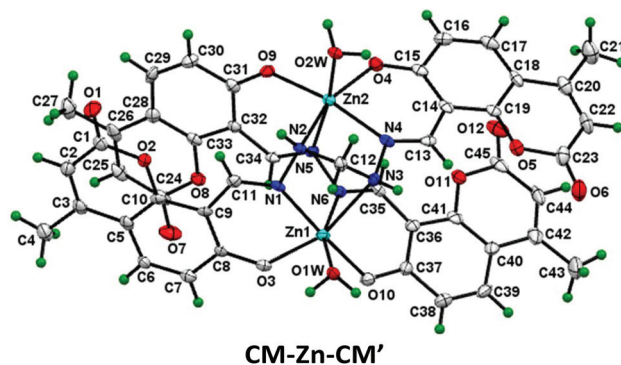


Fig. 4 ORTEP view of a single crystal of zinc complex **CM-Zn-CM'** with displacement ellipsoids at 60% probability.

2.021(3) to 2.129(3) Å and were found to be consistent with other zinc-phenolate complexes.^{18,15b} On the other hand, the Zn–N distances for the three nitrogen donors lie in the range of 2.104(3) to 2.520(3) Å, which are well within the range for analogous zinc complexes.¹⁹ Among the nitrogens, there are two types of donors, *viz.* imine and the amine nitrogens. The bond length with the imine nitrogen is considerably shorter than that with the amine nitrogen. Detailed crystallographic data are given in Table S2, ESI†

In addition to the above routine bond formations, supra-molecular interactions in terms of hydrogen bonding also appear to play an important role in the final architecture of the **CM-Zn-CM'** ensemble. The hydrogen atoms of the coordinated water molecules W(A) and W(B) undergo intermolecular hydrogen bonding with oxygen atoms of the next complex moiety, *i.e.* **CM-Zn-CM'**. This ultimately results in a helical chain architecture. Thus, the two asymmetric units of **CM-Zn-CM'** are interconnected through the O(3)–H(2)WB and O(10)–H(2)WA bonds with separation distances of 1.903 Å and 1.947 Å, respectively (Fig. 5a and b).

Photophysical studies of CMD

In the UV-visible absorption spectrum of a 10 μM ethanolic solution of **CMD**, two broad absorption bands centered at ~350 and ~420 nm were assigned to the π–π* and n–π* transitions, respectively. Upon the addition of Zn²⁺ (0.0 to 17.5 equiv.) as its acetate salt, the former band underwent gradual hyperchromic shifting while the latter band underwent hypo-

chromic shifting along with red shifting of 5 nm. An isosbestic point at 377 nm indicated a chemical interaction between **CMD** and Zn²⁺ (Fig. S27a and S27b, ESI†). Separate additions of 10 equiv. of a number of cations, *viz.* Na⁺, K⁺, Mg²⁺, Ba²⁺, Al³⁺, Ca²⁺, Cr³⁺, Mn²⁺, Fe³⁺, Co²⁺, Ni²⁺, Cu²⁺, Cd²⁺, Hg²⁺ and Pb²⁺, as their chloride salts did not perturb the visible colour or the UV-visible spectral pattern of **CMD** to a significant extent (Fig. S28a and S28b, ESI†). This is somewhat surprising for Cd²⁺ and Hg²⁺ in the sense that both belong to the same group as zinc. The reason for this may be understood in terms of the variations of the physical and chemical behaviour of 3d elements compared to 4d and 5d elements. It is well reported in chemistry textbooks that the 4d elements resemble their 5d counterparts more closely (due to lanthanide contraction) than their 3d congeners. Moreover, the chemosensing action reported here is chemolytic in nature; Zn²⁺ (ionic radius = 74 pm) is more suitable for this due to its smaller size compared to Cd²⁺ and Hg²⁺ (ionic radii = 95 pm and 102 pm, respectively).

To validate the fluorescence turn-on nature of its sensing, the photophysical properties of the probe **CMD** were investigated in ethanol. Free **CMD** upon excitation at 420 nm showed a weak fluorescence signal in the form of a broad band centered at ~560 nm. Upon individual addition of a wide range of metal ions, *viz.* Li⁺, Na⁺, K⁺, Ba²⁺, Mg²⁺, Al³⁺, Ca²⁺, Cr³⁺, Mn²⁺, Fe³⁺, Co²⁺, Ni²⁺, Cu²⁺, Zn²⁺, Cd²⁺, Hg²⁺ and Pb²⁺, as their chloride salts, only Zn²⁺ caused a remarkable fluorescence enhancement at 535 nm with efficient 'turn-on' behavior (Fig. 6 and 7). However, a competition experiment with a number of the

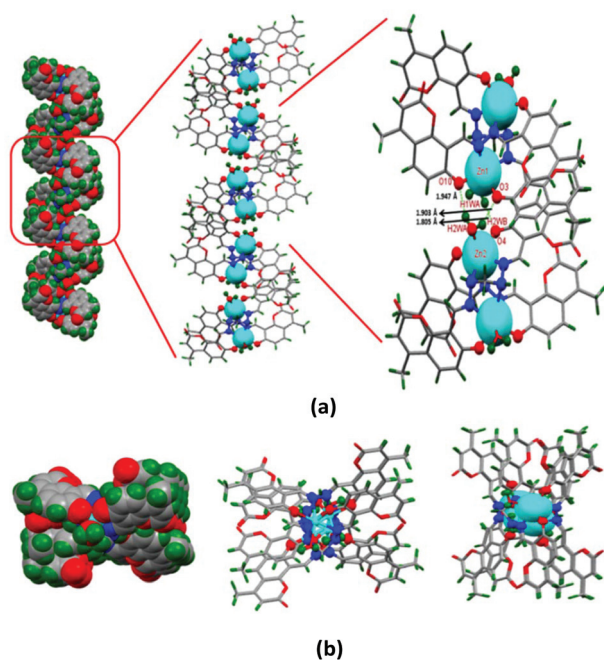


Fig. 5 (a) Weaker intermolecular interactions stabilizing the supramolecular framework and side view of a 1D single-stranded right-handed helical chain along the *c* axis formed due to extension of the intermolecular hydrogen bonding. (b) Upper view of the supramolecular architectures along the *c** axis.

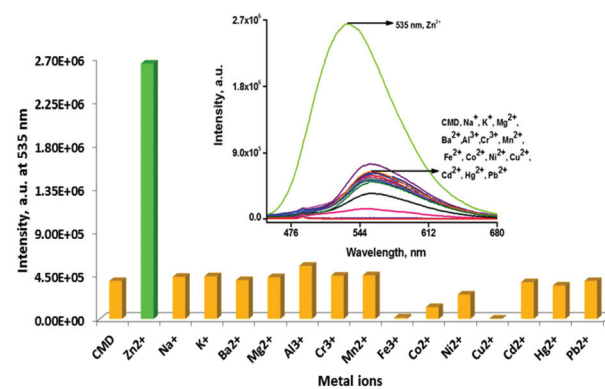


Fig. 6 Relative fluorescence changes of **CMD** (1.0 μM) showing responses to relevant competitive metal ions (10 equiv.) ($\lambda_{\text{ex}} = 420$ nm, $\lambda_{\text{em}} = 535$ nm) with inset showing the fluorescence spectra.

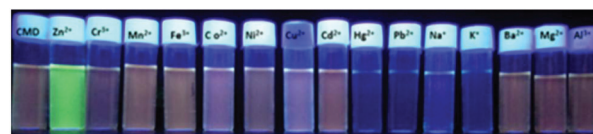


Fig. 7 Visual color changes observed upon addition of different metal ions (10 equiv.) to **CMD** (10 μM) as seen under UV light ($\lambda = 365$ nm).

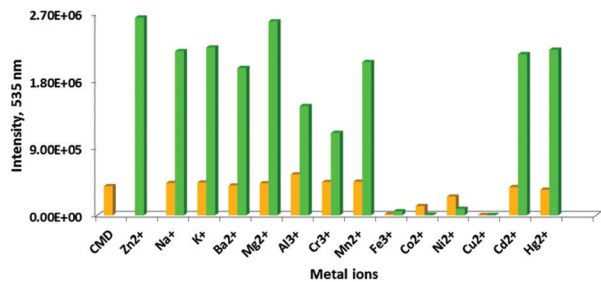


Fig. 8 Effects of most competitive cations on the emission spectrum of CMD + Zn²⁺ at 535 nm.

abovementioned cations was also performed, and it was found that four ions, *viz.* Fe³⁺, Co²⁺, Ni²⁺, and Cu²⁺, did show interference to a considerable extent (Fig. 8).

Fluorescence titration studies were carried out with concomitant additions of Zn²⁺ (0.0 to 44.0 equiv.) to 1.0 μM probe solution. A broad peak appeared around ~535 nm and became fully grown, exhibiting a blue shift of ~20 to 25 nm compared to CMD with ~9 fold enhancement of its fluorescence intensity. At this stage, green fluorescence was observed (Fig. 9). The weakly fluorescent nature of CMD (quantum yield = 0.105) can be understood in terms of intermolecular π-π interactions as well as quenching of the PET phenomenon due to intramolecular hydrogen bonding between the imine nitrogen and phenol (Fig. S29, ESI[†]). The CMD-Zn²⁺ coordination results in two different effects: (i) hampering the intermolecular π-π interactions between CMD molecules, which may result in a blue shift; (ii) coordination of CMD through its nitrogen donors, which is likely to decrease the chance of PET and may be responsible for the hyperchromic shift, *i.e.* intensity magnification, along with enhancement of the quantum yield (0.514). Here, it is worth mentioning that of the number of ratiometric probes reported to date in the literature, only a few of them show Zn²⁺-triggered hypsochromic shifting of the emission wavelength of the receptor.²⁰

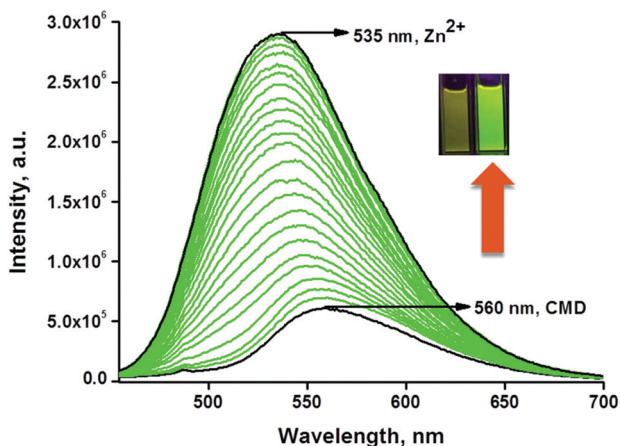


Fig. 9 Fluorescence intensity changes of CMD (1.0 μM) in the presence of Zn²⁺ (0.0 to 44.0 equiv.).

The effects of counter anions were also studied here, and faster kinetics was observed for acetate compared to chloride as the counter anion (Fig. S30, ESI[†]).

Time-dependent intensity measurements of the fluorescence behaviour of CMD (1.0 μM) with respect to Zn²⁺ (10 equiv.) addition revealed that within only 30 seconds, a visible fluorescence change was observed (Fig. S31, ESI[†]). The detection limit (LOD)²¹ calculated from fluorescence titration data of CMD for Zn²⁺ was found to be 3.03×10^{-8} M ($R^2 = 0.998$) with a linearity range of 4.00×10^{-6} to 1.80×10^{-5} M (Fig. S32, ESI[†]).

Interaction mechanism of CMD with Zn²⁺

To obtain a deeper understanding of the interaction patterns of CMD with Zn²⁺, we performed a number of studies, *viz.* ESI-mass spectral studies, ¹H NMR spectroscopy, photophysical studies and single crystal X-ray diffraction studies. The ESI-mass spectrum of CMD in ethanolic medium showed a prominent molecular ion peak *m/z* at 394.3, corresponding to [CMD + H]⁺. However, upon adding 4 equiv. of Zn²⁺ (with acetate as the counter anion), a number of peaks at *m/z* = 380.5 (NSA), *m/z* = 403.5 (CM), *m/z* = 217.4 (ACM), 203.0 (coumarinol) (Fig. S33, ESI[†]), *m/z* = 1138.4 (CM-Zn-CM ensemble), *etc.* (Fig. S34, ESI[†]) were obtained in negative mode. Thus, the mass spectral analysis further supported the dogma of Zn²⁺-triggered hydrolysis of CMD, as we have described above through single crystal X-ray diffraction studies.

¹H NMR studies

In order to substantiate the above findings, we further carried out ¹H NMR titration experiments between CMD and Zn²⁺ in DMSO-*d*₆. A number of new peaks and shifting in the routine peaks of CMD clearly indicated the fragmentation of CMD triggered by Zn²⁺. CMD shows peaks at 12.69 δ ppm and 11.12 δ ppm for its -OH protons and for its aldimine protons at 9.10 δ ppm and 8.81 ppm. Upon addition of Zn(OAc)₂·2H₂O (0.0–5.0 equiv. in DMSO-*d*₆) to CMD, the -OH proton signals shifted upfield and gradually disappeared; the aldimine proton signals of CMD at 9.11 and 8.82 δ ppm were shifted upfield to 8.92 and 8.45 ppm. The peak at 8.45 δ ppm was assigned to NSA and the peak at 8.92 δ ppm was assigned to the aldimine proton of ACM-Hz. A new peak at 9.03 δ ppm appeared and was assigned to the aldimine proton of CM. The peak of the amine group of ACM-Hz appeared at 6.93 δ ppm. Finally, the solution became strongly fluorescent green (Fig. 10). We also carried out ¹H NMR time-dependent experiments and compared the resulting spectra with those of our synthesized compounds. The intermediate ACM-Hz signal appeared at 5 equiv. but disappeared at 10 equiv., probably due to the faster reaction rate at a higher equiv (10 equiv.) of Zn²⁺. These results indicate that the peaks of NSA (formed *in situ*) matched quite well with those of synthesized NSA. However, slight variations in the aldimine protons (8.407 to 9.044 δ ppm) as well as in other protons were observed in the case of CM, probably as a consequence of its binding interactions with Zn²⁺ (available in the reaction medium); the corresponding spectrum is given in ESI, Fig. S35.†

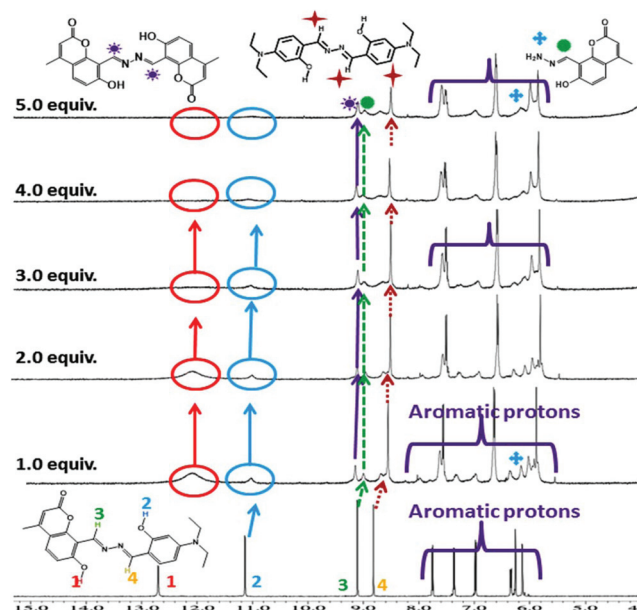


Fig. 10 Partial ^1H NMR spectra showing the gradual changes in the NMR signals upon addition of up to 5 equiv. of Zn^{2+} to **CMD**.

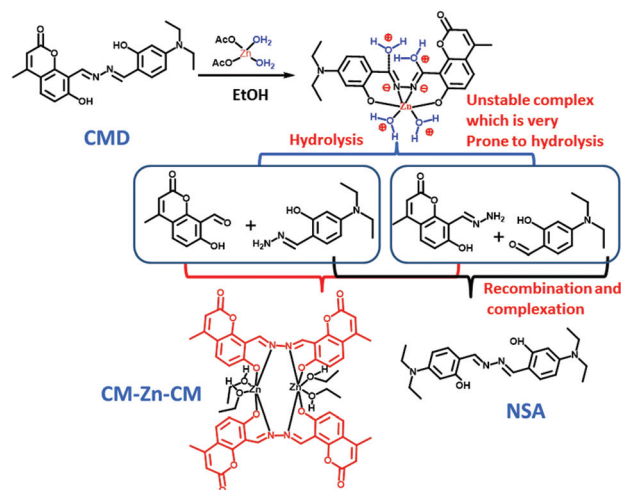
Fluorescence studies were also performed for aldehyde (**ACM**) and amine (**ACM-Hz**), *i.e.* constituents of **CMD**. At the same time, **NSA** and **CM** were also synthesized from their constituents and subjected to physicochemical studies under identical conditions (Fig. S36a, S36b and S37, ESI †). The results were similar to those of the **CM** and **NSA** formed *in situ* during the interaction of **CMD** with Zn^{2+} . Systematic fluorescence studies were also performed with separate additions of Zn^{2+} to all the above molecules under identical experimental conditions. Here, it is worthwhile to mention that the fluorescence characteristics of **NSA** (515 nm) were similar to those of **CMD** solution upon addition of Zn^{2+} . This further fortifies our dogma of scission of **CMD** into **NSA** and other products, as mentioned above.

Thus, comparison of the ^1H NMR titration experiments (Fig. 10 and Fig. S35 †) as well as the fluorescence (S36a and S36b, ESI †) and UV-visible (Fig. S37, ESI †) studies also supported the above mass spectral and X-ray diffraction studies. The Zn^{2+} -triggered hydrolysis of **CMD** as well as the genesis of various recombination products discussed above are conveniently shown in Scheme 2.

A comparison of the scanning electron micrographs (SEM) of **CMD** and its reaction products with Zn^{2+} is shown in Fig. S38, ESI † . The corresponding morphologies of **CMD** prior to (a) and after (b) the addition of Zn^{2+} are shown in Fig. S38, ESI † which indicate a categorical change and finally suggest an interaction between **CMD** and Zn^{2+} .

Practical utility of **CMD**

Detection of Zn^{2+} using a fluorescence spectrophotometer is a cumbersome approach for onsite detection. Hence, to overcome this drawback, we prepared filter paper strips with thin



Scheme 2 Chemodosimetric and supramolecular strategy: hydrolysis of **CMD** in the presence of Zn^{2+} .

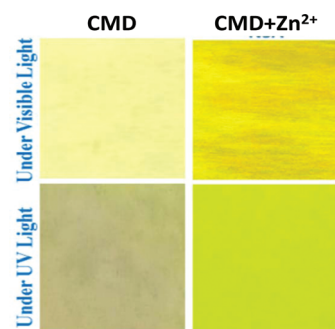


Fig. 11 Chromo-fluorogenic response of test paper strips of **CMD** in the presence of Zn^{2+} .

layer coatings of **CMD**. These strips were prepared by placing filter paper strips (Whatman) in an ethanolic solution of **CMD** (50 micromolar); the strips were dried and used to sense Zn^{2+} . As shown in Fig. 11, when Zn^{2+} was added to the test kits, obvious color changes were observed with Zn^{2+} solution under a 365 nm UV lamp.

Cell culture and fluorescence imaging

Treatment of SiHa cells with 10 μM **CMD** without Zn^{2+} showed very little or no fluorescent signals in the green channel; however, after treatment with Zn^{2+} (5 times higher than the **CMD** concentration), stronger fluorescent signals appeared in the green channel. Similarly, 20 μM **CMD** without Zn^{2+} showed very little green fluorescent signals; however, treatment with Zn^{2+} (5 times higher than the **CMD** concentration) produced very intense green fluorescent signals. In the presence of Zn^{2+} , cells treated with 20 μM **CMD** produced a more intense green signal in comparison to cells treated with 10 μM **CMD**. To identify the nucleus, the cells were treated with DAPI, which can visualize nuclei with a blue fluorescent signal (Fig. 12). Cell

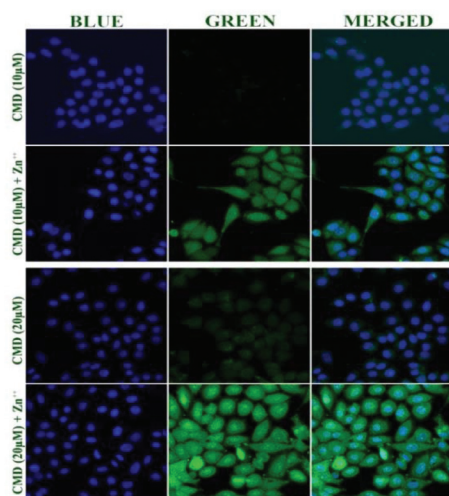


Fig. 12 CMD treatment of SiHa cells showing concentration-dependent (10 μM and 20 μM) increases in the fluorescent green signal in the presence of Zn^{2+} .

viability experiments were also performed in HeLa cells, and the results indicated that with increasing concentration and incubation time of **CMD**, the cells showed minor cytotoxic effects; therefore, we measured the half maximal inhibitory concentration (IC_{50}) range of **CMD**, and it was found to be near 25 μg . Thus, we exposed the cells to **CMD** within the range of its IC_{50} value. These results suggest that **CMD** can be readily used for cellular applications at the indicated dose without causing significant damage to cells (Fig. S39, ESI[†]).

Conclusions

We present here a simple, cost-effective and easy-to-use chemodosimeter for Zn^{2+} in the form of **CMD** synthesized through Schiff base condensation of aldehydes and hydrazine. The very quick response time of **CMD** (only 30 seconds) and its sub-nanomolar limit of detection are additional benefits. The successful imaging of Zn^{2+} in live cells indicate further promise for **CMD**. The various single crystal X-ray structural details add lustre to the academic value of the present study.

Conflicts of interest

There is no conflict of interest among the authors of this paper.

Acknowledgements

A. P. thanks UGC, New Delhi, India, for an SRF fellowship [R./Dev./Sch.(UGC-JRF-410/S-01)] and SKA thanks the CSIR, New Delhi for JRF/SRF [09/013(0475)/2012-EMR-I]. Thanks to Prof. Ida Tiwari for providing the fluorescence machine.

References

- (a) M. Ebadi, F. Perini, K. Mountjoy and J. S. Garvey, *J. Neurochem.*, 1996, **66**, 2121–2127; (b) J. M. Berg and Y. Shi, *Science*, 1996, **271**, 1081–1085; (c) J. Emsley, *Nature's Building Blocks: An A–Z Guide to the Elements*, Oxford University Press, Oxford, 2011.
- (a) K. Velmurugan, A. Raman, D. Don, L. Tang, S. Easwaramoorthi and R. Nandhakumar, *RSC Adv.*, 2015, **5**, 44463–44469; (b) E. L. Que, D. W. Domaille and C. J. Chang, *Chem. Rev.*, 2008, **108**, 1517–1549.
- (a) C. J. Frederickson and A. I. Bush, *BioMetals*, 2001, **14**, 353–366; (b) G. Zhang, H. Li, S. Bi, L. Song, Y. Lu, L. Zhang, J. Yu and L. Wang, *Analyst*, 2013, **138**, 6163–6170; (c) B. L. Vallee and K. H. Falchuk, *Physiol. Rev.*, 1993, **73**, 79–118.
- (a) A. I. Bush, *Trends Neurosci.*, 2003, **26**, 207–214; (b) D. Noy, I. Solomonov, O. Sinkevich, T. Arad, K. Kjaer and I. Sagi, *J. Am. Chem. Soc.*, 2008, **130**, 1376–1383.
- (a) X. Xie and T. G. Smart, *Nature*, 1991, **349**, 521–524; (b) M. P. Cuajungco and G. J. Lees, *Brain Res.*, 1997, **23**, 219–236; (c) K. Falchuk, *Mol. Cell. Biochem.*, 1998, **188**, 41–48; (d) C. J. Frederickson, J.-Y. Koh and A. I. Bush, *Nat. Rev. Neurosci.*, 2005, **6**, 449–462; (e) D. W. Choi and J. Y. Koh, *Neurosci.*, 1998, **21**, 347–375; (f) W. Maret, C. Jacob, B. L. Vallee and E. H. Fischer, *Proc. Natl. Acad. Sci. U. S. A.*, 1999, **96**, 1936–1940.
- (a) A. Q. Truong-Tran, J. Carter, R. E. Ruffin and P. D. Zalewski, *BioMetals*, 2001, **14**, 315–330; (b) B. L. Vallee and K. H. Falchuk, *Physiol. Rev.*, 1993, **73**, 79–118; (c) A. Takeda, *BioMetals*, 2001, **14**, 343–351.
- S. J. Lippard and J. M. Berg, *Principles of Bioinorganic Chemistry*, University Science Books, Mill Valley, CA, 1994.
- (a) S. Gharami, K. Aich, L. Patra and T. K. Mondal, *New J. Chem.*, 2018, **42**, 8646–8652; (b) V. Bhalla, Roopa and M. Kumar, *Dalton Trans.*, 2013, **42**, 975–980; (c) S. H. Jung, K.-Y. Kwon and J. H. Jung, *Chem. Commun.*, 2015, **51**, 952–955.
- (a) Z. Xu, J. Yoon and D. R. Spring, *Chem. Soc. Rev.*, 2010, **39**, 1996–2006; (b) J. Wu, W. Liu, J. Ge, H. Zhang and P. Wang, *Chem. Soc. Rev.*, 2011, **40**, 3483–3495; (c) J. V. Ros-Lis, Ra. Martínez-Mañez, K. Rurack, F. Sancenón, J. Soto and M. Spieles, *Inorg. Chem.*, 2004, **43**, 5183–5185; (d) J. Cheng, X. Ma, Y. Zhang, J. Liu, X. Zhou and H. Xiang, *Inorg. Chem.*, 2014, **53**, 3210–3219.
- (a) Y. Ding, W.-H. Zhu and Y. Xie, *Chem. Rev.*, 2017, **117**, 2203–2256; (b) J. Cao, C. Zhao, X. Wang, Y. Zhang and W. Zhu, *Chem. Commun.*, 2012, **48**, 9897–9899; (c) P.-S. Yao, Z. Liu, J.-Z. Ge, Y. Chen and Q.-Y. Cao, *Dalton Trans.*, 2015, **44**, 7470–7476; (d) R. Mudhulkar, R. R. Nair, I. H. Raval, S. Haldar and P. B. Chatterjee, *ChemistrySelect*, 2017, **2**, 6407–6412.
- (a) X. Dong, J. H. Han, C. H. Heo, H. M. Kim, Z. Liu and B. R. Cho, *Anal. Chem.*, 2012, **84**, 8110–8113; (b) S. Majumder, L. Mandal and S. Mohanta, *Inorg. Chem.*, 2012, **51**, 8739–8749; (c) A. Dhara, N. Guchhait,

- I. Mukherjee, A. Mukherjee and S. C. Bhattacharya, *RSC Adv.*, 2016, **6**, 105930–105939; (d) P. S. Yao, Z. Liu, J. Z. Ge, Y. Chen and Q. Y. Cao, *Dalton Trans.*, 2015, **44**, 7470–7476; (e) R. Singh, A. Gogoi and G. Das, *RSC Adv.*, 2016, **6**, 112246–112252.
- 12 (a) S. Sharma, C. P. Pradeep and A. Dhir, *J. Fluoresc.*, 2016, **26**, 1439–1445; (b) Z. Li, M. Yu, L. Zhang, M. Yu, J. Liu, L. Wei and H. Zhang, *Chem. Commun.*, 2010, **46**, 7169–7171; (c) M.-M. Yu, Z.-X. Li, L.-H. Wei, D.-H. Wei and M.-S. Tang, *Org. Lett.*, 2008, **10**, 1863–1866.
- 13 (a) P. Ding, J. Wang, J. Cheng, Y. Zhao and Y. Ye, *New J. Chem.*, 2015, **39**, 342–348; (b) G. Men, C. Chen, C. Liang, W. Han and S. Jiang, *Analyst*, 2015, **140**, 5454–5458; (c) H. S. Jung, J. H. Han, Y. Habata, C. Kang and J. S. Kim, *Chem. Commun.*, 2011, **47**, 5142–5144; (d) M. Kaur, P. Kaur, V. Dhuna, S. Singh and K. Singh, *Dalton Trans.*, 2014, **43**, 5707–5712.
- 14 (a) K. K. Upadhyay and A. Kumar, *Org. Biomol. Chem.*, 2010, **8**, 4892–4897; (b) V. Kumar, A. Kumar, U. Diwan and K. K. Upadhyay, *Chem. Commun.*, 2012, **48**, 9540–9542; (c) A. Pandey, A. Kumar, S. Vishwakarma and K. K. Upadhyay, *RSC Adv.*, 2016, **6**, 6724–6729.
- 15 (a) R. K. Mishra, K. K. Upadhyay, S. Shukla and R. Mishra, *Chem. Commun.*, 2012, **48**, 4238–4240; (b) N. A. Kumar, V. Kumar, R. Prajapati, S. K. Asthana, K. K. Upadhyay and J. Zhaob, *Dalton Trans.*, 2014, **43**, 5831.
- 16 H. Xiao, K. Chen, D. Cui, N. Jiang, G. Yin, J. Wanga and R. Wang, *New J. Chem.*, 2014, **38**, 2386.
- 17 (a) A. L. Spek, *J. Appl. Crystallogr.*, 2003, **36**, 356–365; (b) A. L. Spek, *Acta Crystallogr.*, 2009, **65**, 148–155.
- 18 (a) P. S. Singh, S. Sivakumar and S. Verma, *Eur. J. Inorg. Chem.*, 2017, 4202–4209; (b) M. A. AlDamen, N. Charef, H. K. Juwhari, K. Sweidan, M. S. Mubarak and D. G. Peters, *J. Chem. Crystallogr.*, 2016, **46**, 411–420.
- 19 (a) H.-W. Chiang, Y.-T. Su and J.-Y. Wu, *Dalton Trans.*, 2013, **42**, 15169–15182.
- 20 (a) V. Bhalla, Roopa and M. Kumar, *Org. Lett.*, 2012, **14**, 2802–2805; (b) L. Xue, G. Li, C. Yu and H. Jiang, *Chem. – Eur. J.*, 2012, **18**, 1050–1054.
- 21 (a) IUPAC, *Spectrochim. Acta, Part B*, 1978, **33**, 242; (b) USEPA, Appendix B to Part 136-Definition and Procedure for the Determination of the Method Detection Limit-Revision 1.11, Federal Register 49(209), 43430, October 26, 1984. Also referred to as “40 CFR Part 136”.